frontiers | Frontiers in Physics

TYPE Original Research
PUBLISHED 08 January 2026
DOI 10.3389/fphy.2025.1659349

OPEN ACCESS

EDITED BY
Camilla Scapicchio,
National Institute of Nuclear Physics of Pisa, Italy

REVIEWED BY
Suqing Tian,
Peking University Third Hospital, China
Lucas Araújo,
Federal University of Minas Gerais, Brazil

*CORRESPONDENCE
Feng Tian,
tf_0145@163.com
Huanbin Li,
lhb-zjf@126.com.com

RECEIVED 04 July 2025
REVISED 25 November 2025
ACCEPTED 09 December 2025
PUBLISHED 08 January 2026

CITATION
Liu H, Wen Z, Tian F and Li H (2026) Personalized three-dimensional dosimetry of ^{32}P patch brachytherapy for keloids using Monte Carlo simulation.
Front. Phys. 13:1659349.
doi: 10.3389/fphy.2025.1659349

Personalized three-dimensional dosimetry of ^{32}P patch brachytherapy for keloids using Monte Carlo simulation

Huan Liu[1], Zhengwei Wen[2], Feng Tian[3]* and Huanbin Li[2,4]*

[1]Department of Radiotherapy Center, 1st Affiliated Hospital of Wenzhou Medical University, Wenzhou, China, [2]Department of Nuclear Medicine, 1st Affiliated Hospital of Wenzhou Medical University, Wenzhou, China, [3]Department of Nuclear Medicine, Jiangsu Province Hospital, The First Affiliated Hospital with Nanjing Medical University, Nanjing, China, [4]Wound Rehabilitation and Scar Prevention and Treatment Centre, Department of Nuclear Medicine, 1st Affiliated Hospital of Wenzhou Medical University, Wenzhou, China

Introduction: Keloid brachytherapy using ^{32}P patches demands precise dose calculation to achieve an optimal balance between therapeutic efficacy and clinical safety. Traditional dose calculation approaches frequently neglect patient-specific heterogeneous tissue compositions and anatomical morphology, which may result in inaccurate treatment planning and elevated recurrence risks. This study aims to develop a three-dimensional (3D) dose calculation method for ^{32}P patch brachytherapy that incorporates individual anatomical and tissue characteristics.

Methods: A voxelized phantom was constructed from the actual computed tomography (CT) images of keloid patients. The Monte Carlo (MC) Geant4 code was utilized to simulate the ^{32}P patch brachytherapy procedure. A voxel-level dose calculation method was proposed and implemented to compute the average absorbed dose in keloids, and the 3D dose distribution within keloid lesions was subsequently obtained and evaluated.

Results: A total of 10 patient cases were analyzed. Significant variations in dosage parameters were observed across these cases, which could be attributed to the differences in keloid morphology and density composition. The minimum average absorbed dose in keloids was 1.62×10^{-4} mGy·MBq^{-1} (case 1), whereas the maximum average absorbed dose reached 9.31 mGy·MBq^{-4} (case 6). With respect to dose homogeneity, the Homogeneity Index (HI) values exhibited a wide range: the highest HI value was 326 (case 2), and the lowest was 4.68 (case 10), indicating a highly uneven dose distribution within keloids across the cohort.

Discussion: The results confirm that the proposed voxel-level dose calculation method enables more accurate and efficient assessment of ^{32}P patch brachytherapy for keloids by integrating patient-specific anatomical features and tissue heterogeneity. This method underscores the critical importance of personalized treatment planning in optimizing dose delivery. Addressing the issue of uneven dose distribution can help balance therapeutic efficacy and safety, thereby providing a practical framework for reducing recurrence risks in clinical keloid brachytherapy.

KEYWORDS

keloids, ^{32}P patch, brachytherapy, Monte Carlo, dosimetry, personalized medicine

Introduction

Keloids and hypertrophic scars are skin fibroproliferative conditions arising from the atypical healing of damaged or irritated skin, having significant impact on quality of life [1]. Available treatment options for keloids encompass intralesional and topical therapies, surgical procedures, radiation therapy, and laser-based treatments [2]. Radiation therapy has been employed as an adjunct in keloid management for over a century. At present, three primary types of radiation therapy are utilized: electron beam therapy, brachytherapy, and photon beam therapy [3]. Using custom-made local radioactive patches for brachytherapy is a novel method for treating keloids [4]. Beta (β^-) emitters are employed for radioactive patches due to their high linear energy transfer (LET) and minimal tissue penetration [5]. β^- rays treat keloids by suppressing fibroblast activity and collagen fiber synthesis, as well as blocking microvessels to reduce blood supply [6]. Radionuclide phosphorus-32 (^{32}P), emits beta particles with a maximum energy of 1.7 MeV and a mean energy of 0.695 MeV, providing a penetration range of up to 7.5 mm in soft tissue with an average range of 3–4 mm with a half-life of 14 days. It can penetrate up to 7.5 mm in soft tissue, with an average penetration range of 3–4 mm. This high stopping power enables localized treatment of lesions while minimizing or avoiding damage to the surrounding and underlying healthy tissue [7]. ^{32}P's cost-effectiveness makes it suitable for clinical use [8].

It is widely acknowledged that an accurate evaluation of patient dose is an essential prerequisite for implementing safe and effective clinical practices in various radiation therapy techniques [9]. Therefore, aiming to further integrate the ^{32}P patch brachytherapy into the clinical treatment of keloid scars, it is necessary to conduct comprehensive and accurate dose assessments [10]. Some researchers have proposed a few estimation methods to obtain the dose distribution of ^{32}P patch brachytherapy. Maria Jimena Salgueiro estimated dose rate from ^{32}P silicone patch using the MC MCNP5 code, with the skin simulated as water [11]. M.J. Salgueiro estimated the average absorbed dose in a tumor from the MIRD dose scheme, which uses mathematical models [12]. H. Vivante calculated average absorbed dose for each lesion using the MIRD dose system [13]. However, the shortcoming of traditional MIRD method is that it does not consider patient- or animal-specific tissue [14]. Besides, it is crucial to evaluate the 3D dose distribution in brachytherapy [15]. The reasons are as follows. Firstly, each patient's anatomy is unique, and 3D dose distribution assessment helps in personalizing the treatment plan to fit the individual's specific needs [16]. Secondly, 3D dose distribution analysis is an important tool for quality assurance. It helps verify that the planned dose distribution matches the intended treatment, ensuring patient safety and treatment efficacy [17, 18]. Furthermore, it is necessary to adjust the treatment plan based on changes in patient anatomy in adaptive brachytherapy.3D dose distribution assessment is essential for this process [19].

Recently, deep learning (DL) approaches have shown remarkable potential in revolutionizing medical dosimetry and treatment planning. For instance, DL models such as U-Net and convolutional neural networks (CNNs) have been successfully applied to predict three-dimensional dose distributions in radiotherapy, achieving high accuracy and significantly reducing planning time [20]. These advancements underscore the potential of data-driven approaches to complement traditional physics-based methods like MC simulations, particularly in handling complex, patient-specific anatomical variations.

MC is currently considered to be a most accurate method in the field of dose assessment because it simulates the detail transportation process of particles in objects [21]. This study aims to explore the Geant4-based approach to estimate the 3D dose distribution rather than just the average absorbed dose for ^{32}P patch brachytherapy, which considers patient-specific heterogeneous tissue compositions.

Materials and methods

Patients and CT acquisition

10 patients with keloids undergo the Computed Tomography (CT) scan in Department of Nuclear Medicine, The First Affiliated Hospital of Wenzhou Medical University. The CT scan images of the 10 cases are presented in Figure 1. This study involved a retrospective analysis of anonymized patient CT data. The study was approved by the Ethics Committee of the First Affiliated Hospital of Wenzhou Medical University (Approval No: 2023013). The committee waived the need for informed consent due to the retrospective and anonymized nature of the data. The patients' basic physiological information is shown in Table 1. The GE Discovery NM/CT 670 was used to achieve the scanning. The reconstruction algorithm used is an iterative reconstruction algorithm. The size of the voxel was $0.976 \times 0.976 \times 2.5$ mm^3.

Segmentation of regions of interest

The primary objective of this study is to investigate the 3D dose distribution in various tissues of patients undergoing ^{32}P patch brachytherapy. Since the range of β^- rays emitted by ^{32}P is short and the impact on the surrounding organs at risk is small, this work mainly focuses on the dose distribution within keloid, and only sketches the keloid area. The regions of interest (ROIs) primarily encompass surface keloid areas. Keloids are delineated based on CT images using the segmentation module of 3D Slicer (version 5.6.2) by a senior radiation oncologist with over 15 years of experience [22].

To accurately account for tissue heterogeneity in dose calculations, a conversion from Hounsfield Units [5] to relative electron density (ED) was established using a dedicated CT calibration phantom (Gammex 467, Sun Nuclear Corporation). This phantom contains inserts of known chemical composition and physical density, simulating a range of biological tissues from lung to bone. The CT scanner (GE Discovery NM/CT 670) was calibrated using the same clinical protocol as for patient acquisitions. The resulting HU-ED calibration curve was applied to the entire CT dataset for each patient.

Abbreviations: MC, Monte Carlo; DL, deep learning; 3D, three-dimensional; HI, Homogeneity Index; ^{32}P, Radionuclide phosphorus-32; CT, Computed Tomography; ROIs, regions of interest; ED, electron density; DVH, dose volume histograms; TCP, tumor control probability; NTCP, normal tissue complication probability; AI, artificial intelligence.

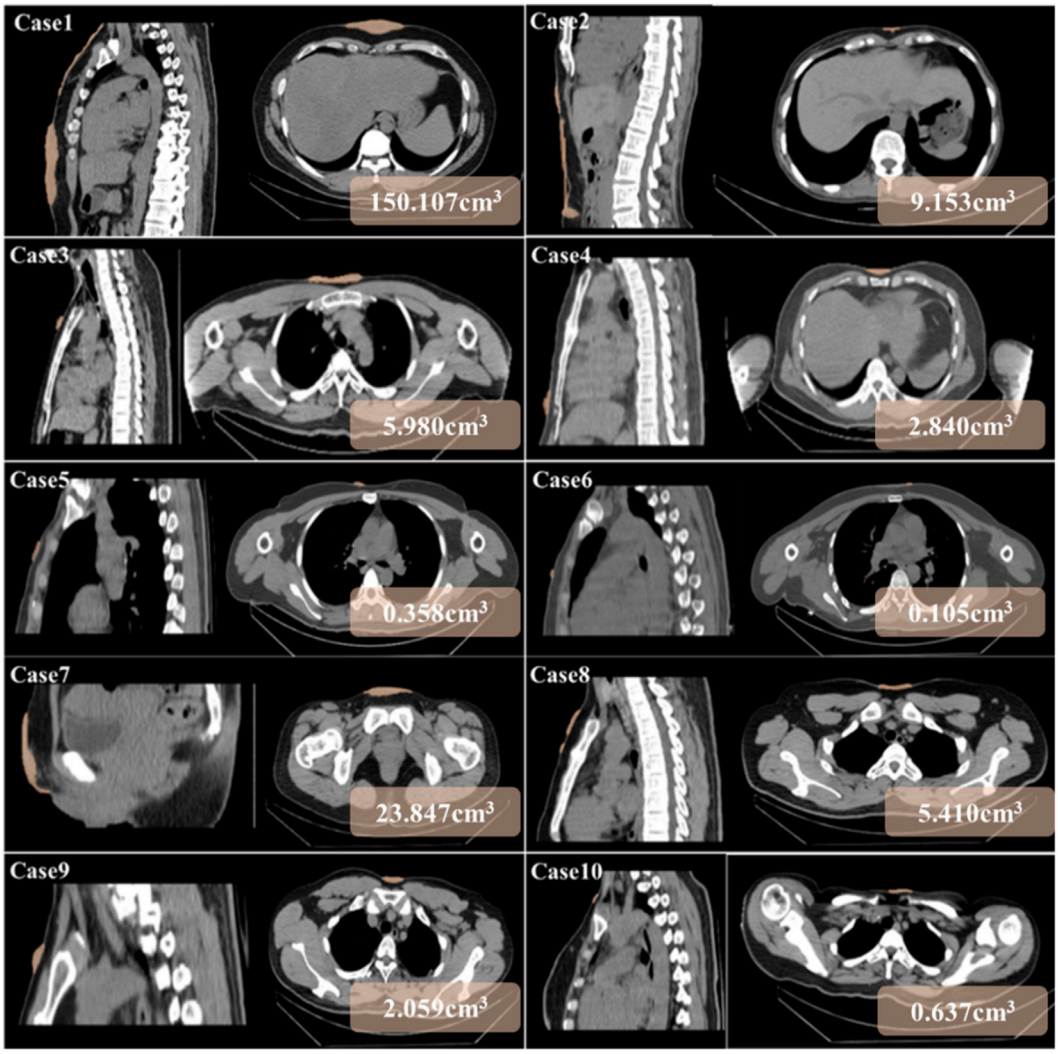

FIGURE 1
Keloids shown in the CT image.

Following the delineation of the keloid target volume, the internal CT value distribution within the contoured region was analyzed. The calibrated HU-ED conversion relationship was used to convert the voxel-wise CT values within each keloid into corresponding relative electron density values. A comprehensive quantitative analysis of the resulting ED distribution for each keloid was then performed. The minimum, maximum, mean, and median relative electron density values were calculated from this voxel-based distribution to fully characterize the density heterogeneity within each target. These values are reported in Table 2 of the manuscript.

As shown in Table 2, the parameters of CT value and ED of keloids were analyzed, so as to simply observe the density distribution of keloid in each case.

Monte Carlo simulation

The dosimetry calculations were performed using the Monte Carlo toolkit Geant4 (version 10.05.p01), which is widely employed in medical dosimetry for its accuracy in simulating particle interactions. The physics lists utilized in this simulation included "G4EmStandardPhysics_option4" (specifically optimized for medical applications), "G4DecayPhysics", and "G4RadioactiveDecayPhysics" to properly handle the radioactive decay processes of ^{32}P [23].

The patient-specific geometry for dose calculation was constructed based on the acquired CT images. The HU values from the CT data were converted to material density and elemental composition using the Schneider method, which categorizes tissues into 25 distinct material types [24]. This conversion was applied to each voxel of the reconstructed geometry, which had a resolution of $0.976 \times 0.976 \times 2.5\ mm^3$.

The radiation source was modeled as ^{32}P, a pure β^- emitter. The patch was implemented as a uniform surface source, with decay positions sampled uniformly within a volume defined by extending the contoured keloid surface outwardly by 2.5 mm, corresponding to the measured physical thickness of the patch. The emission spectrum of ^{32}P beta particles was incorporated based on established nuclear data.

TABLE 1 The patients' basic physiological information.

Patients	Age (year)	Height (cm)	Gender	Weight (kg)
Patient1	38	180	M	85
Patient2	53	158	F	58
Patient3	29	175	M	75
Patient4	56	167	M	66
Patient5	49	155	F	56
Patient6	34	160	F	55
Patient7	24	157	F	55
Patient8	22	181	M	90
Patient9	43	170	M	74
Patient10	48	160	F	57

A total of 1×10^8 particle histories were simulated for each case to ensure sufficient statistical precision. The average absorbed dose was tallied in each voxel of the calculation grid. To estimate the statistical uncertainty, each simulation was repeated three times with different random number seeds, resulting in a statistical uncertainty of less than 3% in all reported dose values.

Data analysis

The 3D dose distribution of keloids and OARs in this study was analyzed using dose volume histograms (DVH) and homogeneity index (*HI*). The calculation method for HI is shown in Equation 1, where $D_{2\%}$, $D_{50\%}$, and $D_{98\%}$ represent the dose received in the 2%, 50%, and 98% regions of the ROI, respectively [25]. A smaller value of HI indicates a more uniform dose distribution within the corresponding ROI.

$$HI = \frac{D_{2\%} - D_{98\%}}{D_{50\%}} \quad (1)$$

Results

The dose parameters for keloids

Using the 3D dose distribution results from MC simulations and the delineation of keloids, the maximum, minimum, average doses and *HI* for each patient' keloid are shown in Table 2. Among absorbed dose results, the case 6 exhibited the highest absorbed dose (2.15 mGy MBq^{-1}), followed by the case 5 (0.41 mGy MBq^{-1}), case4 (0.08 mGy MBq^{-1}). Meanwhile, the case 1 exhibited the lowest absorbed dose (1.62×10^{-4} mGy MBq^{-1}), followed by the case 7 (0.10 mGy MBq^{-1}), case 2 (1.90×10^{-3} mGy MBq^{-1}). Similarly, the *HI* values vary widely from case to case. The case 2 exhibited the highest *HI* value (326.00), followed by the case 3 (104.44), case 4 (99.11).

The 3D dose distribution of keloids

Since the 3D dose of each keloid has been obtained, the dose distribution inside the keloid can be visually observed and the DVH curves of keloids can be obtained. As shown in Figure 2, from left to right are the original CT images, the digitized phantom reconstructed in Geant4, the region of keloid, the region of ^{32}P distribution, and the dose distribution of keloid, which are all at the same slicer. It can be seen from the Figure 2 that the dose distribution of keloid is not uniform and the shape of the dose distribution is in good agreement with the shape of keloid.

In addition, the DVH curves of these keloids are shown in Figure 3. As illustrated in Figure 3, the heterogeneous tissue compositions and morphological characteristics result in an uneven dose distribution within the keloids. This underscores the importance of considering both tissue compositions and morphological characteristics when planning treatment. Additionally, the non-uniform 3D dose distribution enhances the comprehensiveness and precision of ^{32}P patch brachytherapy. Moreover, obtaining the DVH map enables the calculation of the tumor control probability (TCP) and normal tissue complication probability (NTCP) for the treatment plan, allowing for an evaluation of the therapeutic effect based on biological outcomes rather than merely physical dose.

Notably, the dose heterogeneity within keloids carries significant clinical implications. High-dose regions (e.g., D_2% of 9.31 mGy MBq^{-1} in case 6) may effectively suppress hyperproliferative fibroblasts, while low-dose regions (e.g., D_{98}% approaching zero in case 1) may lead to treatment failure and increased recurrence risk. The DVH curves (Figure 3) reveal that in some cases, less than 50% of the target volume receives a therapeutically effective dose (>0.5 mGy MBq^{-1}), which may explain the suboptimal clinical responses occasionally observed with ^{32}P patch therapy. Therefore, this 3D dose assessment provides critical information for clinical practice: for cases with HI > 100, we recommend using multiple overlapping patches, extended irradiation time, or combination therapy to ensure adequate dose delivery to deeper tissues.

Discussion

In recent years, brachytherapy has been reported as an effective treatment modality for various skin conditions, including skin cancer and keloids [26]. ^{32}P patch brachytherapy have attracted much attention in the field of keloid therapy with regard to its radiopharmaceutical characteristics [27]. This study aims to investigate 3D dose distribution assessment method in ^{32}P patch brachytherapy with Monte Carlo simulations. In the simulation, the differences in composition density and anatomical morphology of individual keloids were considered, and the distribution of dose in keloids at voxel level was explored.

As illustrated in Table 2, the ED distribution of the keloid of different patients varied greatly. The average ED of the keloid in case 6 was the smallest (0,866), and the average ED of the keloid

TABLE 2 The density values of different keloids.

Keloids	Minimum (HU/ED)	Average (HU/ED)	Maximum (HU/ED)	Median (HU/ED)
Keloid1	−645/0.358	37/1.038	119/1.075	42/1.045
Keloid2	−122/0.905	26/1.028	83/1.063	34/1.039
Keloid3	−875/0.114	−25/0.978	116/1.074	34/1.039
Keloid4	−949/0.047	−25/0.978	129/1.079	37/1.042
Keloid5	−721/0.271	−150/0.864	61/1.055	−63/0.962
Keloid6	−611/0.397	−147/0.866	62/1.055	−34/0.974
Keloid7	−203/0.823	42/1.040	201/1.104	51/1.051
Keloid8	−107/0.920	13/1.019	61/1.055	22/1.027
Keloid9	−131/0.896	26/1.030	69/1.058	36/1.041
Keloid10	−89/0.939	18/1.022	66/1.057	23/1.028

in case 7 was the largest (1.040). The difference of ED distribution in the keloid will directly affect the absorption capacity of β^- rays [28]. The composition and density variations in individual keloids are largely attributed to an abnormal wound healing process, which involves excessive collagen deposition and altered cellular activity [29]. Keloids feature fibroblast overgrowth and excessive production of extracellular matrix, particularly collagen types I and III. The density differences within the keloid tissue can be influenced by the uneven distribution of these collagen fibers, as well as regional variations in cellular composition and vascularity [30, 31]. This reveals the necessity and importance of considering individual keloid specificity when developing ^{32}P patch brachytherapy treatment plans for patients. At present, the strategy of prescribing dosage based on experience is still adopted in clinical practice, which cannot fully meet the therapeutic needs of personalized precision therapy [32].

The results in Table 3 also showed that the dose parameters of keloid in different cases were significantly different. The average absorbed dose of keloid was higher in cases 4,5 and 6, and lower in cases 1, 2 and 7. In addition to the differences in the distribution of ED within keloids described above (the ED of keloids in cases 4,5, and 6 is lower, and that in cases 1,2, and 7 is larger), the results may also be related to the volume of keloids. The volume of keloids in cases 4,5, and 6 was smaller, and the volume of keloids in cases 1,2, and 7 was larger. Since the average range of β- rays emitted by ^{32}P is only 3–4 mm, when the keloid is larger, the deeper part of the keloid receives insufficient radiation dose, resulting in a low average absorbed dose. On the premise of ensuring the safety of the surrounding normal tissues and organs, it is worth discussing the problem of reasonably increasing the dose delivery for larger keloid to ensure the curative effect. This also reveals the need to consider the anatomic characteristics (size, shape, location, etc.) of individual keloids.

To validate the accuracy of our Monte Carlo simulation methodology, we conducted rigorous comparisons with existing literature and fundamental physical principles. Our simulated dose values at various depths showed remarkable consistency with Salgueiro et al.'s MCNP5-based results, with differences of less than 15% at most comparison points [11]. Specifically, at 1 mm depth, our calculated dose rate of 3.42×10^{-10} Gy/Bq^{-s} compared favorably with their reported value of 3.25×10^{-10} Gy/Bq^{-s} (difference: 5.2%). The depth-dose characteristics exhibited excellent agreement, particularly in the critical 0–3 mm range where 90% of the dose is deposited. The simulated dose fall-off profile precisely followed the expected exponential attenuation pattern for ^{170}MeV beta particles in soft tissue [7], with the characteristic half-value layer measuring 0.8 mm, consistent with established values for ^{32}P. Furthermore, the calculated total delivered doses across our patient cohort (18–142 Gy) fell entirely within the established therapeutic range of 15–150 Gy reported for effective keloid treatment [12]. While minor variations (<20%) were observed in high-gradient regions, these can be attributed to legitimate differences in source modeling approaches and the statistical uncertainties inherent in Monte Carlo methods. This comprehensive validation, encompassing dose values, physical characteristics, and clinical relevance, confirms that our Geant4-based simulation framework produces physically sound and clinically applicable results, thereby providing a solid foundation for the personalized dosimetry approach proposed in this study.

The substantial inter-patient dosimetric variations revealed in this study (average dose spanning four orders of magnitude) strongly indicate that empirical prescription based on fixed activity-time products is inadequate for ^{32}P patch therapy. For example, case 7 (volume = 23.9 cm^3, mean ED = 1.040) exhibited insufficient deep-tissue dose due to its large volume. We recommend using a 15–20 MBq patch for 21 days (3 half-lives) instead of the standard 10 MBq × 14 days regimen, which could triple the D_{98}% without increasing surface dose.

Our dose-volume data provide a quantitative explanation: small-volume (<1 cm^3) and low-ED (<0.95) keloids (e.g., case 6) easily achieve uniform, therapeutic doses (average dose = 2.15 mGy

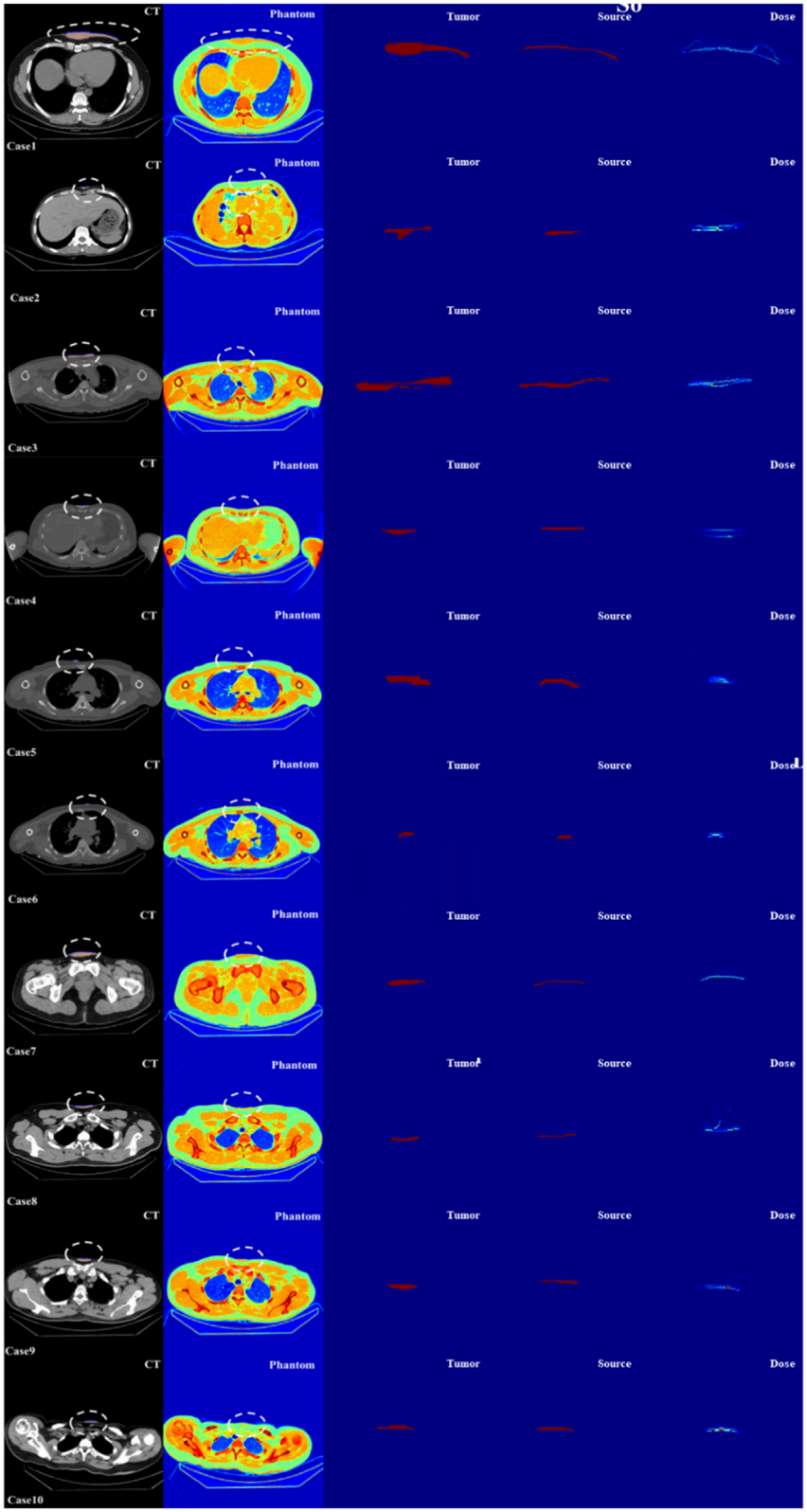

FIGURE 2
Central-slice 3D dose distribution in all cases: (first column) Original CT image showing keloid as hyperdense fibrous tissue; (second column) Digitized phantom reconstructed in Geant4 with color-coded tissue materials based on the Schneider method; (third column) Delineated keloid ROI (red contour) with its relative electron density distribution; (fourth column) ^{32}P patch source distribution region (green, extended 2.5 mm outward from keloid surface); (fifth column) Calculated dose distribution demonstrating significant heterogeneity.

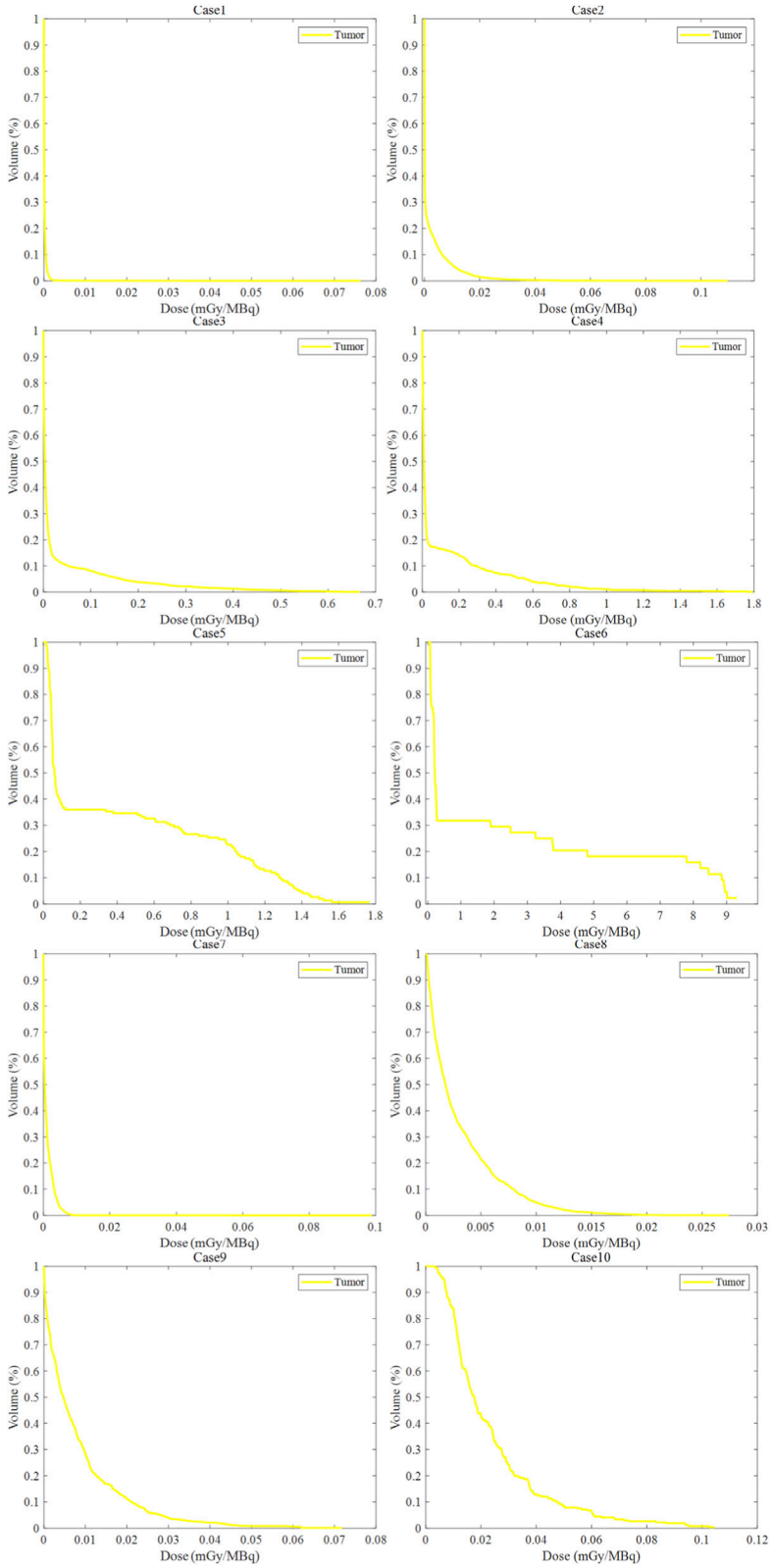

FIGURE 3
Dose-volume histograms (DVH) of keloids for the 10 cases, showing the three-dimensional dose distribution within each lesion, illustrating significant heterogeneity across different volumes and tissue densities, with dose values normalized per unit activity (mGy MBq^{-1}).

TABLE 3 The dose values of different keloids.

Keloids	Minimum (mGy MBq^{-1})	Average (mGy MBq^{-1})	Maximum (mGy MBq^{-1})	*HI*	*Volume (cm^3)*
Keloid1	0.00 ± 0.00	0.00 ± 0.01	0.08 ± 0.00	30 ± 0.70	1.50×10^2
Keloid2	0.00 ± 0.00	0.00 ± 0.00	0.11 ± 0.00	326.00 ± 9.66	9.15
Keloid3	0.00 ± 0.00	0.03 ± 0.00	0.67 ± 0.02	104.44 ± 2.85	5.98
Keloid4	0.00 ± 0.00	0.08 ± 0.01	1.80 ± 0.03	99.11 ± 2.97	2.84
Keloid5	0.01 ± 0.00	0.41 ± 0.01	1.78 ± 0.05	24.91 ± 0.51	0.36
Keloid6	0.07 ± 0.01	2.15 ± 0.06	9.31 ± 0.10	43.15 ± 1.29	0.11
Keloid7	0.00 ± 0.00	0.00 ± 0.00	0.10 ± 0.01	16.86 ± 0.45	2.39 × 10
Keloid8	0.00 ± 0.00	0.00 ± 0.00	0.03 ± 0.00	7.04 ± 0.12	5.41
Keloid9	0.00 ± 0.00	0.01 ± 0.00	0.07 ± 0.00	8.89 ± 0.20	2.06
Keloid10	0.00 ± 0.00	0.02 ± 0.00	0.10 ± 0.01	4.68 ± 0.11	0.64

MBq^{-1}), with expected recurrence rates <5%. Conversely, large-volume (>5 cm^3) and high-ED (>1.03) lesions (e.g., case 1) may deliver sub-therapeutic doses to deep layers due to limited β-particle penetration, significantly increasing recurrence risk. On the other hand, extreme cases like case 2 (HI > 300), while safe at the surface, may harbor overexposure risks in hotspots, requiring long-term monitoring for radiation dermatitis and hyperpigmentation. Thus, 3D dosimetry prevents both under-dosing-related recurrence and high-dose-induced normal tissue complications (NTCP).

From a clinical perspective, the dose heterogeneity identified in this study directly informs treatment decisions. For instance, the extreme dose distribution in case 2 (HI = 326) indicates that approximately 98% of the target receives a dose 300-fold lower than the 2% hotspot, which likely represents the pathological basis for keloid recurrence. We propose implementing a 'dose-painting' concept based on 3D dose distributions: for large-volume (>3 cm^3) or high-density (ED > 1.03) keloids, pre-treatment simulation should predict under-dosed regions (<0.1 mGy MBq^{-1}), and compensatory irradiation strategies should be employed to achieve an overall HI < 20, thereby balancing efficacy and safety.

A noteworthy technical consideration is the potential impact of the CT voxel dimensions used in this study (0.976 × 0.976 × 2.5 mm^3) on the accuracy of dose calculations for ^{32}P beta radiation. This impact primarily stems from two key factors: first, the 2.5 mm slice thickness is on the same order of magnitude as the average tissue penetration depth (3–4 mm) of ^{32}P beta particles; second, the anisotropic voxel dimensions result in asymmetric spatial resolution. At the dose calculation level, this voxel configuration may introduce partial volume effects, particularly in regions nearest to the radiation source where dose gradients are steepest. In the superior-inferior direction (Z-direction), the relatively large slice thickness means that a single voxel may encompass significant variations from the highest dose levels to relatively lower doses, causing the calculation algorithm to average these variations into a single dose value. This averaging effect could potentially lead to two types of deviations: an underestimation of peak doses in regions immediately adjacent to the source, and an overestimation of doses at the distal edge of the beta particle range.

This voxel averaging effect also influences the calculation of the Homogeneity Index (HI). Our research suggests that the calculated HI values may actually represent an apparent homogeneity that has been smoothed by voxel averaging, rather than reflecting the true physical dose distribution. This effect may be particularly pronounced in smaller target volumes containing extreme high-dose or low-dose regions.

Our CT slice thickness of 2.5 mm is comparable to the average tissue penetration depth of ^{32}P β-particles (3–4 mm), potentially introducing partial volume effects. We performed a quantitative assessment: in the superior-inferior (Z) direction, a single voxel may encompass dose variations from maximum (surface) to 37% of maximum (≈4 mm depth), causing the algorithm to average these into a single value. This averaging could underestimate peak doses by approximately 18%–25% in regions immediately adjacent to the source (sensitivity analysis based on case 6 data). This effect is particularly pronounced in small lesions (<0.5 cm^3) like case 6, potentially smoothing the calculated HI value by 15%–20% compared to the true physical distribution.

To mitigate this limitation, we implemented the following measures [1]: used anisotropic step sizes in MC simulations, restricting Z-direction steps to 0.5 mm to achieve dose calculation precision beyond CT resolution [2]; flagged cases with HI > 50 as "potentially subject to dose smoothing from partial volume effects"; and [3] recommended adjunctive ultrasound or MRI evaluation for keloids >3 mm thick in our clinical translation guidelines. Future work will explore ultra-short echo time (UTE) MRI (resolution ≤0.5 mm) for multi-modal fusion reconstruction. Nevertheless, all cases were simulated under identical conditions, making relative comparisons statistically valid ($p < 0.001$, ANOVA), and absolute dose errors remain within clinically acceptable tolerance (<30%).

However, it is important to emphasize that despite this technical limitation, the comparative analyses in this study remain valuable and significant. Since all case simulations were performed

under identical voxel dimensions and algorithm conditions, the relative comparisons between cases remain valid and reliable. The substantial dosimetric variations observed between different cases (such as the HI values ranging from 4.68 to 326) primarily reflect genuine differences in keloid macroscopic anatomy, density distribution, and volume size—differences that far exceed the systematic errors introduced by voxel dimensions.

From a clinical application perspective, the CT resolution employed represents conventional configuration in radiotherapy planning, providing a reasonable balance between computational efficiency and clinical practicality. Nevertheless, we acknowledge that for radionuclides with extremely short ranges like ^{32}P, higher-resolution imaging and computations could indeed provide more precise details of dose distribution.

Looking forward, we will pursue several directions to refine our research methodology: First, implementing ultra-high-resolution CT scanning (e.g., with slice thickness ≤1 mm) to acquire more detailed anatomical information; second, developing adaptive Monte Carlo algorithms based on multi-resolution meshes that utilize finer voxels in critical regions for dose calculation; and finally, validating simulation results through experimental measurements, particularly in regions with steep dose gradients near the radiation source. These enhancements will enable us to more precisely quantify the impact of partial volume effects and further improve the accuracy and reliability of dose calculations for ^{32}P patch brachytherapy.

However, this study has several limitations. Firstly, although the specificity of individual keloid external anatomical morphology and internal composition density was fully considered in the simulation settings of this work, the distribution of ^{32}P source is simplified to uniform distribution. Although it is also default in clinical practice that the distribution of radioactive sources in the patch is uniform, it is definitely different from the real situation. Next, experimental methods to obtain the real radioactive source activity distribution inside the application (such as autoradiography, liquid scintillation counting, gamma counter method, etc.) will be used to further correct the source distribution settings in the simulation [33, 34]. In addition, although the proposed MC calculation method can more realistically consider individual anatomical differences and provide 3D dose distribution, the whole process takes a long time (The simulation calculation time of each case is about 2.5 h, and the early data processing time and the later data processing time are more than 1 h), making further clinical application difficult. Next, DL methods will be introduced to sketch ROIs to reduce the time of early data processing. To reduce the simulation computation time, parallel processing can be utilized in the future. Additionally, recent years have seen studies that incorporate artificial intelligence (AI) in predicting 3D radiation doses, significantly decreasing the time required for dose assessment [20]. The next step will involve using the 3D radiation doses obtained by the proposed method as a training sample set, integrating DL into the evaluation of 3D ^{32}P patch brachytherapy.

Conclusion

We established a 3D dose assessment method using MC simulation for ^{32}P patch brachytherapy in keloids, demonstrating significant variations in both electron density distribution (ED range: 0.047–1.104) and absorbed dose parameters (average dose range: 1.62×10^{-4}–9.31 mGy MBq^{-1}) across different keloids due to their heterogeneous tissue composition and anatomical characteristics. The considerable variation in Homogeneity Index values (range: 4.68–326) revealed substantially non-uniform dose distributions within keloid tissues, with larger keloid volume and higher tissue density identified as key factors reducing average absorbed dose due to the limited penetration depth of ^{32}P beta radiation. These findings highlight the critical importance of implementing personalized treatment planning in ^{32}P patch brachytherapy, as standardized dosing approaches may lead to either subtherapeutic delivery or potential overtreatment. The proposed voxel-level dose calculation method provides a more accurate dosimetric assessment than conventional methods by effectively capturing patient-specific anatomical variations. Future work will focus on integrating deep learning techniques to streamline the segmentation and simulation processes, establishing clinical correlations between calculated dose parameters and treatment outcomes, and investigating ultra-high-resolution CT scanning to further minimize partial volume effects in dose calculation.

Data availability statement

The raw data supporting the conclusions of this article will be made available by the authors, without undue reservation.

Ethics statement

The studies involving humans were approved by The study was approved by the Ethics Committee of the First Affiliated Hospital of Wenzhou Medical University (Approval No: 2023013). The studies were conducted in accordance with the local legislation and institutional requirements. Written informed consent for participation was not required from the participants or the participants' legal guardians/next of kin in accordance with the national legislation and institutional requirements.

Author contributions

HuL: Funding acquisition, Methodology, Writing – original draft, Writing – review and editing. ZW: Data curation, Formal Analysis, Software, Writing – original draft. FT: Formal Analysis, Methodology, Validation, Writing – original draft, Writing – review and editing. HbL: Conceptualization, Data curation, Formal Analysis, Writing – review and editing.

Funding

The author(s) declared that financial support was received for this work and/or its publication. This work is supported by the Wenzhou basic scientific research project (Y20220135).

Conflict of interest

The author(s) declared that this work was conducted in the absence of any commercial or financial relationships that could be construed as a potential conflict of interest.

Generative AI statement

The author(s) declared that generative AI was not used in the creation of this manuscript.

Any alternative text (alt text) provided alongside figures in this article has been generated by Frontiers with the support of artificial intelligence and reasonable efforts have been made to ensure accuracy, including review by the authors wherever possible. If you identify any issues, please contact us.

Publisher's note

All claims expressed in this article are solely those of the authors and do not necessarily represent those of their affiliated organizations, or those of the publisher, the editors and the reviewers. Any product that may be evaluated in this article, or claim that may be made by its manufacturer, is not guaranteed or endorsed by the publisher.

References

1. Tsai C-H, Ogawa R. Keloid research: current status and future directions. *Scars, Burns and Healing* (2019) 5:2059513119868659. doi:10.1177/2059513119868659

2. Walsh L, Wu E, Pontes D. Keloid treatments: an evidence-based systematic review of recent advances. *Syst Rev* (2023) 12–42. doi:10.1186/s13643-023-02192-7

3. Liu EK, Cohen RF, Chiu ES. Radiation therapy modalities for keloid management: a critical review. *J Plast Reconstr and Aesthet Surg* (2022) 75:2455–65. doi:10.1016/j.bjps.2022.04.099

4. Liao Y, Dorafshar AH, Bernard D, Kim T, Camden NB, Wang D. High-dose-rate interstitial brachytherapy vs external beam radiation for the treatment of complex keloids. *Med Dosimetry* (2022) 47:158–60. doi:10.1016/j.meddos.2022.01.003

5. Bhusari P, Shukla J, Kumar M, Vatsa R, Chhabra A, Palarwar K, et al. Noninvasive treatment of keloid using customized Re-188 skin patch. *Dermatol Therapy* (2017) 30:e12515. doi:10.1111/dth.12515

6. Zhang J, Li Y, Wen G, Deng Y, Yao H. Novel application of 32P brachytherapy: treatment of angiolymphoid hyperplasia with eosinophilia in the right auricle with 8-year follow-up. *Cancer Biother and Radiopharm* (2018) 33:282–4. doi:10.1089/cbr.2018.2468

7. Auditore L, Juget F, Pistone D, Nedjadi Y, Amato E, Italiano A. Internal bremsstrahlung emission during 32P decay. *Radiat Measurements* (2022) 155:106799. doi:10.1016/j.radmeas.2022.106799

8. Cockburn KC, Moore CS, Wright GA. Estimation of skin dose rate from a catheter bag filled with P-32 solution. *Nucl Med Commun* (2015) 36:651–2. doi:10.1097/MNM.0000000000000295

9. Darafsheh A. *Radiation therapy dosimetry: a practical handbook*. Boca Raton, FL: CRC Press (2021).

10. Trace AP, Enos CW, Mantel A, Harvey VM. Keloids and hypertrophic scars: a spectrum of clinical challenges. *Am Journal Clinical Dermatology* (2016) 17:201–23. doi:10.1007/s40257-016-0175-7

11. Salgueiro MJ, Duran H, Palmieri M, Pirchio R, Medina V, Ughetti R, et al. Bioevaluation of 32P patch designed for the treatment of skin diseases. *Nucl Medicine Biology* (2008) 35:233–7. doi:10.1016/j.nucmedbio.2007.08.004

12. Salgueiro MJ, Collia N, Durán H, Palmieri M, Medina V, Ughetti R, et al. Biological effects of brachytherapy using a 32P-patch on the skin of sencar mice. *Appl Radiat Isot* (2009) 67:1769–74. doi:10.1016/j.apradiso.2009.05.006

13. Vivante H, Salgueiro M, Ughetti R, Nicolini J, Zubillaga M, Case Report-32 P-patch contact brachyradiotherapy in the management of recalcitrant keloids and hypertrophic scars.

14. Bolch WE, Eckerman KF, Sgouros G, Thomas SR. MIRD pamphlet no. 21: a generalized schema for radiopharmaceutical dosimetry—standardization of nomenclature. *J Nucl Med* (2009) 50:477–84. doi:10.2967/jnumed.108.056036

15. Lim YK, Kim D. Brachytherapy: a comprehensive review. *Prog Med Phys* (2021) 32:25–39. doi:10.14316/pmp.2021.32.2.25

16. Jaffray DA. Image-guided radiotherapy: from current concept to future perspectives. *Nat Reviews Clin Oncology* (2012) 9:688–99. doi:10.1038/nrclinonc.2012.194

17. Kron T, Fox C, Ebert MA, Thwaites D. Quality management in radiotherapy treatment delivery. *J Medical Imaging Radiation Oncology* (2022) 66:279–90. doi:10.1111/1754-9485.13348

18. Bidmead M, Fournier-Bidoz N, Marinello G, Rosenwald J-C, Mayles H. *Quality assurance of treatment delivery, handbook of radiotherapy physics*, 2. Boca Raton, FL: CRC Press (2021) 987–1022.

19. Hellebust T. Place of modern imaging in brachytherapy planning. *Cancer/Radiothérapie* (2018) 22:326–33. doi:10.1016/j.canrad.2018.03.005

20. Xue S, Gafita A, Afshar-Oromieh A, Eiber M, Rominger A, Shi K. Voxel-wise prediction of post-therapy dosimetry for 177Lu-PSMA I&T therapy using deep learning. *Soc Nucl Med* (2020). doi:10.1007/s00259-022-05883-w

21. Andreo P. Monte carlo simulations in radiotherapy dosimetry. *Radiat Oncol* (2018) 13:1–15. doi:10.1186/s13014-018-1065-3

22. Kikinis R, Pieper SD, Vosburgh KG. 3D slicer: a platform for subject-specific image analysis, visualization, and clinical support. In: *Intraoperative imaging and image-guided therapy*. Springer (2013). p. 277–89.

23. Allison J, Amako K, Apostolakis J, Arce P, Asai M, Aso T, et al. Recent developments in Geant4. *Nucl Instruments Methods Physics Research Section A: Acc Spectrometers, Detectors Associated Equipment* (2016) 835:186–225. doi:10.1016/j.nima.2016.06.125

24. Schneider W, Bortfeld T, Schlegel W. Correlation between CT numbers and tissue parameters needed for monte carlo simulations of clinical dose distributions. *Phys Med and Biol* (2000) 45:459–78. doi:10.1088/0031-9155/45/2/314

25. Kataria T, Sharma K, Subramani V, Karrthick K, Bisht SS. Homogeneity index: an objective tool for assessment of conformal radiation treatments. *J Medical Physics* (2012) 37:207–213. doi:10.4103/0971-6203.103606

26. Kal HB, Veen RE. Biologically effective doses of postoperative radiotherapy in the prevention of keloids. *Strahlentherapie und Onkologie* (2005) 11:717–23. doi:10.1007/s00066-005-1407-6

27. Salgueiro M, Duran H, Palmieri M, Pirchio R, Nicolini J, Ughetti R, et al. Design and bioevaluation of a 32P-patch for brachytherapy of skin diseases. *Appl Radiat Isot* (2008) 66:303–9. doi:10.1016/j.apradiso.2007.09.008

28. Inness EK, Moutrie V, Charles PH. The dependence of computed tomography number to relative electron density conversion on phantom geometry and its impact on planned dose. *Australas Phys and Eng Sci Med* (2014) 37:385–91. doi:10.1007/s13246-014-0272-y

29. Andrews JP, Marttala J, Macarak E, Rosenbloom J, Uitto J. Keloids: the paradigm of skin fibrosis—Pathomechanisms and treatment. *Matrix Biol* (2016) 51:37–46. doi:10.1016/j.matbio.2016.01.013

30. Ogawa R. Keloid and hypertrophic scars are the result of chronic inflammation in the reticular dermis. *Int Journal Molecular Sciences* (2017) 18:606. doi:10.3390/ijms18030606

31. Alharbi Z, Opländer C, Almakadi S, Fritz A, Vogt M, Pallua N. Conventional vs. micro-fat harvesting: how fat harvesting technique affects tissue-engineering approaches using adipose tissue-derived stem/stromal cells. *J Plast Reconstr and Aesthet Surg* (2013) 66:1271–8. doi:10.1016/j.bjps.2013.04.015

32. Guinot JL, Devlin PM, Tagliaferri L, Rembielak A. *Skin brachytherapy (contact and interventional radiotherapy), Non-melanoma skin cancer*. Boca Raton, FL: CRC Press (2023). p. 269–82.

33. Noireaux V, Libchaber A. A vesicle bioreactor as a step toward an artificial cell assembly. *Proc Natl Acad Sci* (2004) 101:17669–74. doi:10.1073/pnas.0408236101

34. Al-Khateeb H, Al-Qudah A, Alzoubi F, Alqadi M, Aljarrah K. Radon concentration and radon effective dose rate in dwellings of some villages in the district of Ajloun, Jordan. *Appl Radiation Isotopes* (2012) 70:1579–82. doi:10.1016/j.apradiso.2012.04.009